HOKKAIDO UNIVERSITY

Title	Physico-chemical Behavior of Hydrogen Sulfide Induced by Reactions with H and D Atoms on Different Types of Ice Surfaces at Low Temperature
Author(s)	Oba, Yasuhiro; Tomaru, Takuto; Kouchi, Akira et al.
Citation	Astrophysical journal, 874(2), 124 https://doi.org/10.3847/1538-4357/ab0961
Issue Date	2019-04-01
Doc URL	https://hdl.handle.net/2115/77214
Rights	This is an author-created, un-copyedited version of an article accepted for publication/published in Astrophysical journal. IOP Publishing Ltd is not responsible for any errors or omissions in this version of the manuscript or any version derived from it. The Version of Record is available online at 10.3847/1538-4357/ab0961.
Type	journal article
File Information	Astrophysical journal874(2)_124-.pdf

Hokkaido University Collection of Scholarly and Academic Papers : HUSCAP

Physico-chemical behavior of hydrogen sulfide induced by reactions with H and D atoms on different types of ice surfaces at low temperatures

Short title: Reactions of H_2S with H and D atoms on ices

Yasuhiro Oba*, Takuto Tomaru, Akira Kouchi, and Naoki Watanabe

Institute of Low Temperature Science, Hokkaido University, N19W8, Kita-ku, Sapporo, Hokkaido 060-0189 JAPAN

* Corresponding author: oba@lowtem.hokudai.ac.jp

Abstract

To elucidate the physico-chemical behavior of hydrogen sulfide (H_2S) on icy grains in dense molecular clouds, we investigated the surface reactions of solid H_2S with H and D atoms in low-temperature laboratory experiments. We confirmed that H_2S was lost from the surface by reaction with H atoms via chemical desorption. We found no strong association between the effective desorption cross section and the ice structure (porous amorphous, non-porous amorphous, or crystalline) or temperature (10–30 K). At 10 K,

the reaction rate constant for the H–D substitution of solid H_2S with D atoms almost matched that for the D–H substitution of solid D_2S with H atoms. The present experimental results clearly suggest that the observed abundances of H_2S and its deuterated isotopologues (HDS and D_2S) in the interstellar medium are controlled, at least partly, by surface reactions on interstellar icy grains.

Key words: astrochemistry — ISM: molecules — ISM: clouds

1. Introduction

Hydrogen sulfide (H_2S) is one of the most primitive sulfur-bearing molecules detected in the interstellar medium (ISM). Since its first detection in W3 and NGC 7538, and five other Galactic regions (Thaddeus et al. 1972), H_2S has been detected in the gas phases of various interstellar sources, such as cold dark clouds (Minh et al. 1989), diffuse clouds (Neufeld et al. 2015), hot cores (Hatchell et al. 1998), star-forming regions (Wakelam et al. 2004), low-mass protostars (van Dishoeck et al. 1995; Vastel et al. 2003), and a protoplanetary disk (Phuong et al. 2018). By contrast, the presence of solid-state H_2S remains debatable. Geballe et al. (1985) reported solid H_2S in the infrared spectrum of a high-mass protostar W33A. However, because of the faint

infrared feature of the possible H_2S band at 3.9 μm, the presence of solid-state interstellar H_2S in this source is inconclusive and is not universally accepted in the astrochemical community (e.g., Garrod et al. 2007; Jiménez-Escobar & Muñoz Caro 2011).

As the observed interstellar abundance of H_2S cannot be explained by gas-phase synthesis alone, it is thought to be mainly formed by successive additions of H atoms to S atoms on icy grains (Millar et al. 1986; Millar & Herbst 1990):

$$S + H \rightarrow HS, \quad (1)$$

$$HS + H \rightarrow H_2S. \quad (2)$$

As reactions (1) and (2) are barrierless, H_2S is easily formed on icy grains even at extremely low temperatures (~10 K). When H_2S remains on the grains, it can further react with H atoms as follows:

$$H_2S + H \rightarrow HS + H_2, \quad (3)$$

which has a moderate activation barrier of approximately 1500 K (Lamberts & Kästner 2017). The HS radicals revert to H_2S via reaction (2). Garrod et al. (2007) attributed the abundant gas-phase H_2S to desorption of the H_2S formed by reaction (2). This mechanism, here called *chemical desorption*, is also known as reactive desorption. Chemical desorption is a non-thermal desorption mechanism that operates through the

heat of exothermic reactions on grains. Chemical desorption was pioneered by the modeling community to explain the gas-phase abundances of molecules derived from icy grains at low temperatures (Garrod et al. 2007; Cuppen et al. 2017). Recently, it has been experimentally demonstrated on several molecules (Dulieu et al. 2013; He et al. 2017; Chuang et al. 2018; Oba et al. 2018). Using Fourier-transform infrared (FTIR) spectroscopy, we recently quantified the chemical desorption of H_2S and H atoms reacting on the surface of amorphous solid water (ASW) at 10 K (Oba et al. 2018). In that experiment, the H_2S abundance was reduced through the repetition of reactions (2) and (3). Clearly, chemical reactions play a dominant role in desorption of H_2S and/or HS into the gas phase.

To further elucidate the physico-chemical behavior of H_2S at low temperatures, we now react H_2S with not only H atoms but also D atoms. From the experimental results, we deduce a possible mechanism for the deuterium enrichment of HS in the ISM and the dependence of chemical desorption on physical parameters such as the temperature and structure of the ice.

2. Experiments

2.1. Apparatus

In all experiments, we applied the surface-reaction monitoring system used in our previous study (Oba et al. 2018). The main components are an ultrahigh vacuum chamber, a reflection–absorption type FTIR, a quadrupole mass spectrometer (QMS), a gold-coated substrate connected to a helium cryostat, and an atomic source chamber. The substrate temperature is controllable between 5 and 280 K inclusive. The base pressure in the chamber is of the order 10^{-8} Pa.

2.2. Experimental procedure

2.2.1. H_2S + H

H_2S was reacted with H atoms on the surfaces of three types of H_2O ice: porous (p-) ASW, non-porous (np-) ASW, and polycrystalline water ice (c-H_2O). The p-ASW was produced by the vapor-deposition of gaseous H_2O through a capillary plate inclined at 45° to the surface normal at 10–30 K. The np-ASW and c-H_2O were formed similarly, but at different deposition surface temperatures (90 and 140 K, respectively). The substrates of the np-ASW and c-H_2O samples were cooled to 10 K after deposition. The thickness of each ice was adjusted to approximately 30 monolayers (MLs, where 1 ML = 1×10^{15} molecules cm^{-2}). The deposition rate of the ice was ~2 ML $minutes^{-1}$. Gaseous H_2S was deposited through the same capillary plate onto the H_2O ice at 10–30

K for p-ASW and at 10 K for np-ASW and c-H_2O. The H_2S thickness (~0.7 ML) was estimated from the peak area and the band strength of the S–H stretching band at ~2570 cm^{-1} (8.3×10^{-18} cm $molecules^{-1}$; Fathe et al. 2006). The H_2S deposition rate was ~1 ML $minutes^{-1}$. Hydrogen atoms were produced by dissociating H_2 molecules in a microwave-induced H_2 plasma in a Pyrex tube. The produced atoms were transferred through a series of polytetrafluoroethylene and aluminum (Al) tubes, which thermalized them to ~100 K through multiple collisions with the inner wall of the Al tube (100 K). Following the method proposed by Oba et al. (2014a), the H-atom flux was estimated as 5.7×10^{13} atoms cm^{-2} s^{-1}. The reaction was monitored in situ by FTIR for up to 3 hr. After exposure to H atoms, the abundance of H_2S remaining on the ice was measured in temperature-programmed desorption (TPD) experiments using the QMS. As a blank experiment, the deposited H_2S (~0.7 ML) was exposed to H_2 molecules for the same duration. Neither reaction nor desorption was confirmed in the blank, even at 30 K. The FTIR measurements, TPD experiments, and blank experiments were performed as described in the following section, unless otherwise noted.

2.2.2. H_2S + D

Approximately 0.7 ML of solid H_2S was prepared on the surface of p-ASW,

np-ASW, or c-H_2O at 10 K. The preparation method has been described in the previous section. The ice thickness was adjusted to 30 ML, and the deposited H_2S was exposed to D atoms for up to 2 hr at 10 K. The D atoms were produced by dissociating D_2 molecules in a microwave-induced D_2 plasma, which was cooled to 100 K before reaction with H_2S on the ice surface. The estimated flux of D atoms was 2.5×10^{14} atoms cm^{-2} s^{-1}.

2.2.3. D_2S + H

Gaseous D_2S was deposited on the surface of porous amorphous deuterated water (D_2O, hereafter denoted as p-ASW-d). The p-ASW-d was 30 ML thick at 10 K, and the solid D_2S thickness (~0.7 ML) was estimated from the peak area and the reported band strength of the S–D stretching band of amorphous D_2S at 1860 cm^{-1} (4.3×10^{-18} molecules cm^{-1}; Fathe et al. 2006). If the D_2O is substituted with H_2O, the D_2S deposition can be accompanied by hydrogen–deuterium exchange between H_2O and D_2S in the present experimental set up, causing possible misinterpretations of the results. Therefore, we applied D_2O instead of H_2O in this experiment. The deposited D_2S was exposed to a flux of H atoms (1.1×10^{14} atoms cm^{-2} s^{-1}) for 2 hr at 10 K.

Note that the reported band strengths of solid H_2S and D_2S were obtained by

the transmission absorption spectroscopy (Fathe et al. 2006), while we used these values in the reflection absorption spectroscopy, which may cause some errors on the estimate of column densities. In the cases of amorphous H_2O and solid CO, for example, we found that the difference in the estimated column densities between transmission and reflection methods was within a factor of two (Oba et al. 2009). Despite such potential errors on the column densities of solid H_2S and D_2S, we consider that the obtained parameters reported in the next section are acceptable since we focus on the variations in the relative abundances of solid H_2S and D_2S.

3. Results and Discussion

3.1. H_2S + H on p-ASW at 10–30 K

Figure 1 shows an FTIR spectrum of solid H_2S deposited on p-ASW at 20 K, and the difference spectra after exposure to H atoms for 5 and 30 minutes. The peak at ~2570 cm^{-1} was assigned to the S–H stretching band of solid H_2S (Fathe et al. 2006). After exposure to H atoms, the magnitude of the S–H stretching band reduced, but no growth of infrared absorption bands resulting from other sulfur-bearing species was observed. In addition, no desorption of sulfur-bearing species except H_2S was confirmed in the TPD experiment. These results clarify that solid H_2S was lost by

chemical desorption from the surface. The same phenomenon was demonstrated at 10 K by Oba et al. (2018), and at 30 K in the present study (spectrum not shown).

Figure 2 shows the relative abundances of solid H_2S on p-ASW prepared at 10, 20 and 30 K as functions of atom exposure time. At each temperature, the abundance of solid H_2S gradually decreased and eventually settled at ~60% of the initial abundance in the 10 and 20 K experiments, and at ~30% in the 30 K experiment. The presence of the unreacted fraction is probably due to the presence of H_2S adsorbed in the potentially deep sites on ice, where the reaction of H_2S with H atoms may be suppressed significantly (Oba et al. 2018). H_2S loss from the ice was also confirmed in the TPD experiment (Fig. 3). The peaks at 95, 145, and 160 K are attributed to desorption of most of the weakly bound H_2S from the top of the ASW surface, the H_2S emitted by the molecular volcano process, and the co-desorption of H_2S and H_2O, respectively (Collings et al. 2004; Oba et al. 2018).

The effective cross section of the chemical desorption of H_2S, assuming that the H_2S desorbs by a single H-atom injection process, is given by Oba et al. (2018):

$$\Delta[H_2S]_t/[H_2S]_0 = \alpha(1-\exp(-\sigma\varphi t)), \quad (4)$$

where $\Delta[H_2S]_t$ and $[H_2S]_0$ represent the abundance variations of the solid H_2S at time t and the initial H_2S abundance, respectively, and α, σ, and φ are the saturation values of

the desorption fraction, the effective cross section of chemical desorption, and the atom flux, respectively. By fitting the plots in Figure 2 to Equation (4) and dividing the obtained fitting parameter by the H-atom flux, the effective cross sections σ of the chemical desorption from p-ASW at 10, 20 and 30 K were determined as $(2.1 \pm 0.2) \times 10^{-17}$, $(1.3 \pm 0.1) \times 10^{-17}$, and $(9.6 \pm 1.2) \times 10^{-18}$ cm^2, respectively. Note that the obtained effective cross section can be considered as the lower limit of the actual desorption cross section since the incident H-atom flux does not always cause chemical desorption. This suggests that chemical desorption is only slightly more efficient at lower temperatures than at higher temperatures. However, it should be noted that Equation (4) may oversimplify the elementary processes of H atoms on ice. Because the surface number density of H atoms markedly drops at around 20 K because of the low sticking coefficient, fewer H atoms should contribute to the surface reactions as the temperature increases under the same flux of atoms. The observed small difference in the effective cross section implies that the efficiency of chemical desorption per reactive event increases at higher temperatures.

By contrast, the saturation value of the desorption fraction clearly depends on the reaction temperature. At 30 K, the desorption fraction was approximately half that at 10 and 20 K (Fig. 2). We first consider the effect of the solid H_2S structure on the

reactivity, as reported previously (Hama et al. 2014). Even at low coverage, some fraction of the H_2S may aggregate at the ice surface. The solid structure may also depend on the deposition temperature. Hama et al. (2014) found that H atoms react less readily with crystalline benzene than with amorphous benzene, which they attributed to geometric constraints between the two solid phases. However, the crystallization temperature in the H_2S case exceeds 65 K (Fathe et al. 2006), much higher than the temperatures of the present experiment. Furthermore, we confirmed that approximately 60% of the solid H_2S was also released from the ice surface by chemical desorption when the sample prepared at 30 K was exposed to H atoms at 10 K. We thus conclude that the differences in solid structure arising from the sample preparation temperature do not affect the desorption fraction. We propose that the amount of non-desorbed H_2S fraction is related to the residence time of the H atoms, which varies with temperature. Although the structures of the p-ASW and H_2S surfaces should be considerably similar at temperatures below 30 K, the number of adsorption sites at which an H atom can remain sufficiently long for reactions (2) and (3) should decrease with increasing temperature. In particular, reaction (3), which should occur via tunneling because of the moderate energy barrier (Lamberts & Kästner 2017), requires a long residence time of H atoms at the reaction sites. At 30 K, most of the H atoms are transiently desorbed

from the surface, and only the H_2S at relatively deeper adsorption sites can contribute to reactions (3) and (2), which may in part results in chemical desorption. Moreover, the H_2S peak at 95 K in the TPD spectra of the 30 K experiment (Figure 3(b)), which is attributed to weakly bound H_2S at the ASW surface, shows no signature of chemical desorption after exposure to atoms. Meanwhile, the depleted peaks at 140 and 160 K indicate chemical desorption of H_2S and/or HS. By contrast, the 95 K peak in the 20 K experiment was reduced after the atom exposure, confirming that even the weakly bound H_2S was desorbed by reactions with H atoms at 20 K.

3.2. H_2S + H on p-ASW, np-ASW, and c-H_2O at 10 K

Figure 4 shows the relative abundances of solid H_2S after exposure to H atoms on the three kinds of ices at 10 K. Solid H_2S was lost from all surfaces by chemical desorption. The saturation values of the desorbed fractions were considerably similar on the p-ASW and np-ASW surfaces (~60% of the initial abundance), whereas on c-H_2O, the desorbed fraction saturated at approximately 80% of the initial abundance. The different abundances on ASW and c-H_2O can be explained by the flatter surface of c-H_2O than ASW, admitting a larger number of H-atom accessible sites.

Fitting the plots in Figure 4 by Equation (4), the effective desorption cross

sections on the p-ASW, np-ASW, and c-H_2O ices at 10 K were obtained as (2.1 ± 0.2) × 10^{-17}, (1.6 ± 0.2) × 10^{-17}, and (9.4 ± 0.7) × 10^{-18} cm^2, respectively. The effective desorption cross section of H_2S did not strongly depend on ice structure, suggesting that H_2S was effectively desorbed from all ice structures under the present experimental conditions.

3.3. H_2S + D on p-ASW, np-ASW, and c-H_2O at 10 K

When solid H_2S was reacted with D atoms on p-ASW, np-ASW and c-H_2O, the H_2S abundance decreased and deuterated sulfides (HDS and D_2S) were formed. These species were evidenced by the appearance of their S–D stretching band at 1860 cm^{-1} (Figure 5). In our previous study, we confirmed that deuterated sulfides were formed on p-ASW at 10 K by the following H–D substitution reactions (Oba et al. 2018):

$$H_2S + D \rightarrow HS + HD, \quad (5)$$

$$HS + D \rightarrow HDS, \quad (6)$$

$$HDS + D \rightarrow DS + HD, \quad (7)$$

$$DS + D \rightarrow D_2S. \quad (8)$$

Clearly, the deuterated sulfides formed via reactions (5)–(8) on the np-ASW and c-H_2O surfaces as well. At 10 K, reactions (5) and (7) must proceed by quantum tunneling

(Lamberts & Kästner 2017), whereas reactions (6) and (8) have no activation barrier, and therefore easily proceed at this temperature. The absorption features observed at ~2500 cm^{-1} (Fig. 5) may be due to the O-D stretching band of D_2O, which was introduced from the D-atom source. Since the column density of the accumulated D_2O was negligible (~0.02 ML after 20 minutes), it would not affect the reactivity of solid H_2S with D atoms on the H_2O ice. Figure 6 shows the relative peak areas of the S–H stretching band (Area[S–H]$_t$) after exposure to D atoms on the three kinds of H_2O ice, normalized by the initial peak area of the S–H stretching band of H_2S (Area[S–H]$_0$). As singly deuterated sulfide (HDS), which contributes to the S–H stretching band in the same region, is produced through the above reaction pathways, the variations in Area[S–H]$_t$ should be constrained by not only the decrease of H_2S but also the increase and decrease of HDS. Hence, to clarify the whole kinetics of the H–D substitution of H_2S, we must quantify the abundance variations in both H_2S and HDS. However, HDS is difficult to quantify in the IR spectra because its H–S stretching band overlaps that of H_2S at ~2570 cm^{-1}. Although the peak positions of the bending band should vary among the isotopologues, such peaks were not observed in the present study, because of the low abundances of the isotopologues (<0.7 ML) on the ice.

To simplify the discussion on the kinetics of the H–D substitution reactions, we

assume that the temporal variations in the Area[S–H]$_t$/Area[S–H]$_0$ values during the D-atom exposure are dominated by the rate of reaction (5). That is, we assume that HDS immediately converts to D_2S and does not contribute to the observed H–S band. Although the estimation is rough, the obtained parameters should be useful for discussing the kinetics of the entire reaction system. Under such conditions, the abundance variation of H_2S in Figure 6 can be described by the following rate equation:

$$d[H_2S]/dt = -k_{HD}[D][H_2S], \quad (9)$$

where [D] represents the abundance of D atoms on the ices, and k_{HD} is the rate constant of reaction (5). Integrating Equation (9), we get

$$\Delta[H_2S]_t/[H_2S]_0 = \alpha(1-\exp(-k't)), \quad (10)$$

where $\Delta[H_2S]_t$ and $[H_2S]_0$ represent the H_2S abundance variation at time t and the initial H_2S abundance, respectively, and k' (= k_{HD}[D]) is the effective rate constant of reaction (5), which is equivalent to that of H–D substitution of H_2S. Fitting the plots in Figure 6 to Equation (10), the effective rate constants on the p-ASW, np-ASW, and c-H_2O surfaces were calculated as $(5.7 \pm 0.4) \times 10^{-1}$, $(3.0 \pm 0.3) \times 10^{-1}$, and $(3.4 \pm 0.4) \times 10^{-1}$ min^{-1}, respectively. Since the numbers of adsorption sites on np-ASW and c-H_2O are extremely similar, and lower than on p-ASW (Stevenson et al. 1999; Kimmel et al. 2001), the surface number density of D atoms (denoted [D]) may be larger on p-ASW

than on other kinds of ices. If k_{HD} is independent of ice structure, k' will be larger on p-ASW than on other ice surfaces. By this argument, Hidaka et al. (2007) explained the different effective rate constants of CO + H on p-ASW and c-H_2O. The present study suggests that the same argument is applicable to other reaction systems. The obtained values are of the same order of magnitude as the H–D substitution reaction rates of other molecules (CH_3OH, H_2CO, CH_3NH_2, CH_3CH_2OH, and CH_3OCH_3) investigated under similar experimental conditions (e.g., surface temperature and atom flux) (Nagaoka et al. 2007; Hidaka et al. 2009; Oba et al. 2014b, 2016a,b).

Figure 7 shows the peak areas of the S–D stretching band of the deuterated sulfides at 1860 cm^{-1} after exposure to D atoms on different ice surfaces. On all surfaces, the peak intensity of the S–D stretching band drastically increased after short-term exposure to D atoms, was maximized at ~10 min, and decreased with further exposure to the atoms. The earlier part of the exposure was dominated by the formation of deuterated sulfides from H_2S by the H–D substitution reaction; in the latter part, the deuterated sulfides were removed from the ice surfaces by chemical desorption, described by reactions (7) and/or (8). An additional reaction (11) might also contribute to the loss of D_2S by chemical desorption (Oba et al. 2018):

$$D_2S + D \rightarrow DS + D_2. \qquad (11)$$

The formed DS radicals further react with D atoms to regain D_2S (reaction 8), which may partly desorb during its formation. As clarified in the plots, the desorption of deuterated sulfides was more suppressed on p-ASW than on np-ASW and c-H_2O, possibly reflecting the variable numbers and natures of the adsorption sites on different ice surfaces.

3.4. D_2S + H on p-ASW-d

Figure 8 shows the FTIR spectrum of solid D_2S (~0.7 ML) prepared on the p-ASW-d surface (~30 ML) at 10 K, along with the difference spectra after exposure to H atoms for 3, 5 and 20 min. The peak intensity of the S–D stretching band at ~1860 cm^{-1} decreased with increasing atom-exposure time, suggesting that the interactions with H atoms reduced the D_2S abundance on the surface. Similar to the H–D substitution reactions of solid H_2S, we expect that D_2S exposed to H atoms undergoes successive D abstraction and H addition reactions, forming hydrogen-substituted sulfides (HDS and H_2S) as follows:

$$D_2S + H \rightarrow DS + HD, \quad (12)$$

$$DS + H \rightarrow HDS, \quad (13)$$

$$HDS + H \rightarrow HS + HD, \quad (14)$$

$$HS + H \rightarrow H_2S. \quad (15)$$

Note that reaction (15) is identical to reaction (2). As reactions (13) and (15) are radical–radical reactions with no activation barrier, they easily proceed on the ice surface, even at 10 K. However, reactions (12) and (14), with activation barriers of ~1800 and ~1500 K, respectively (Lamberts & Kästner 2017), can proceed only by quantum tunneling at 10 K. The formed hydrogen-substituted sulfides are not clarified at ~2570 cm^{-1} in the difference spectra, as their S–H band is obscured by variations in the O–D stretching band of p-ASW-d in the same region (Fig. 8b). We preliminary confirmed that the S–H stretching band of pure solid D_2S grows under exposure to H atoms on a gold-coated metal substrate at 10 K (Fig. 8c). Based on these results, we are confident that the D–H substitution of D_2S proceeds after interactions with H atoms, even on p-ASW-d.

Figure 9 plots the relative peak area of the S–D stretching band versus the exposure time to H-atoms (the results of H_2S after exposure to D atoms on p-ASW are also shown for comparison). Assuming that the intermediate species HDS contributes insignificantly to the decrease of the S–D stretching band, the plots in Figure 9 approximately show the variations in the relative abundance of D_2S dissociated by reaction (12) only. Under those conditions, the kinetic parameters of the D–H

substitution reactions can be obtained by fitting the plots of Figure 9 to the following equation:

$$\Delta[D_2S]_t/[D_2S]_0 = \alpha(1-\exp(-k_{DH}[H]t)), \quad (16)$$

where $\Delta[D_2S]_t$ and $[D_2S]_0$ represent the variation in the D_2S abundance at time t and the initial D_2S abundance, respectively, and k_{DH} and [H] represent the rate constant of reaction (12) and the surface number density of H atoms on the ice, respectively. As [H] cannot be measured under the present experimental conditions, k_{DH} cannot be isolated from the fitting parameter. Instead, the fitting parameter $k_{DH}[H]$ (= k'') is defined as the effective rate constant of reaction (12), equivalent to that of D–H substitution of D_2S. Accordingly, by comparing k'' and k', we can discuss the possible isotope effects on the H–D and D–H substitution reactions.

The effective rate constant k'' was calculated as $(1.4 \pm 0.1) \times 10^{-1}$ minutes^{-1}, approximately one-quarter that of k' (5.7×10^{-1} minutes). According to Kuwahata et al. (2015), the number density ratio of D and H atoms ([D]/[H]) on the p-ASW surface in the present flux regime (~1–2 × 10^{14} atoms cm^{-2} s^{-1}) is approximately 3. Therefore, the isotope effect on the H–D and D–H substitution reactions (k_{HD}/k_{DH}) can be calculated by rearranging the relationship $k'/k'' = k_{HD}[D]/k_{DH}[H]$ as follows:

$$k_{HD}/k_{DH} = 1/3 \times k'/k'' = 1.35.$$

Lamberts and Kästner (2017) theoretically estimated the isotope effect on the same reaction system at 55–240 K. Assuming that these reactions proceed by quantum tunneling, the reaction rate is temperature-independent, especially in the low-temperature regime. Hence, the relative reaction rate at 55 K would not significantly differ from that at lower temperatures (such as 10 K). Lamberts and Kästner (2017) calculated the values of k_{HD} and k_{DH} at 55 K (1.07×10^6 $s^{-1}$and 7.50×10^5 s^{-1}, respectively, in Table S4 in their article), resulting in the k_{HD}/k_{DH} ratio as $(1.07 \times 10^6)/(7.50 \times 10^5) = 1.43$, which excellently agrees with our experimental value.

4. Astrochemical Implications

4.1 Chemical desorption of H_2S

Recently, we demonstrated that chemical desorption removes H_2S from interstellar icy grains more effectively than photodesorption, releasing H_2S and/or HS into the gas phase even at 10 K (Oba et al. 2018). However, it remains to be clarified whether chemical desorption effectively proceeds when H_2S and H atoms react on np-ASW, which is thought to be representative of H_2O structures in dense clouds, as so-called dangling OH bands have not been detected in astronomical observations (Smith et al. 1989). Minissale et al. (2016) explored chemical desorption from np-ASW

in laboratory studies and proposed that several molecules could desorb during their formation. The present results similarly showed that H_2S can be released into the gas phase via chemical desorption on np-ASW (Fig. 4). Moreover, the effective desorption cross section (an indicator of desorption efficiency) is equivalent to that of p-ASW.

In our previous study, we estimated the desorption efficiency per incident H atom as 5.4×10^{-3}, under an H-atom flux of 1.3×10^{14} atoms cm^{-2} s^{-1} (Oba et al. 2018). For comparison, we here calculate the desorption efficiency per incident H atom (in molecules $atoms^{-1}$) under the same experimental conditions (i.e. on p-ASW at 10 K). Dividing the H_2S decrease during the initial 10 minutes (2.3×10^{14} molecules cm^{-2}) by the H-atom fluence over the same duration (3.4×10^{14} atoms cm^{-2}), we obtain 6.7×10^{-3}, similar to the previous value. Although this argument is not verifiable under the present experimental conditions, if the H_2S desorbs via reaction (2) only, the desorption efficiency would be double that of the calculated one ($\sim 1.3 \times 10^{-2}$), because the number of available H atoms in reaction (2) is at most half the total atom fluence. If the calculated value is equivalent to the lower limit of the desorption efficiency per reactive event, as defined in chemical modeling studies (Garrod et al. 2007; Furuya et al. 2013), then our value exceeds the value 8×10^{-3} commonly assumed in models (Wakelam et al. 2017; K. Furuya, 2018, private communication). Furthermore, the experimentally

1 determined lower limit is probably lower than that in actual interstellar clouds, because
2 most of the H atoms landed on the ice surface would recombine in the laboratory
3 experiment, lowering the number of H atoms available for reactions with H_2S and HS.
4 Hence, we again conclude that H_2S can be released from icy grains via chemical
5 desorption at higher efficiencies than hitherto expected. Accordingly, H_2S desorption
6 should be an important source of gaseous H_2S in cold dense clouds, regardless of the ice
7 structures on the grains.
8
9 4.2. Contribution to deuterated sulfides in the ISM
10 Deuterated sulfides have been detected in the ISM (van Dishoeck et al. 1995;
11 Vastel et al. 2003). The observed abundances of HDS and D_2S relative to H_2S are 10^{-1}
12 toward IRAS16293–2422 (van Dishoeck et al. 1995) and of the order of 10^{-2} toward
13 class 0 sources and dense cores (Vastel et al. 2003). The deuteration levels of sulfide
14 species are significantly higher than the cosmic abundance of D atoms (~1×10^{-5};
15 Linsky 2003) and the deuteration levels of ISM water (HDO/H_2O ~3×10^{-2}, D_2O/H_2O ~
16 1×10^{-3}, Coutens et al. 2012, 2014; Vastel et al. 2010). The different deuteration levels
17 of H_2S and H_2O are probably attributable to their different deuteration pathways: H_2O is
18 deuterated during its formation process only (Oba et al. 2012; Taquet et al. 2013),

whereas H_2S, once formed on grains, can also be deuterated through H–D substitution processes. Therefore, the deuteration level of H_2S can potentially exceed the atomic D/H ratio in the environment. It is widely recognized that H–D substitution reactions on grains enrich the deuterium contents of various interstellar molecules, such as methanol and formaldehyde (Nagaoka et al. 2007; Hidaka et al. 2009; Taquet et al. 2013). In particular, the heavily deuterated signature of methanol toward class 0 protostars (e.g., $CH_2DOH/CH_3OH > 0.4$, Parise et al. 2006) reflects the extremely low occurrence of D–H substitution in methanol, meaning that its deuteration level remains high (Nagaoka et al. 2007). In other words, once deuterated methanol such as CH_2DOH and CHD_2OH is formed through the H–D substitution reactions of CH_3OH, it never returns to the original non-deuterated methanol, which explains the significant deuterium enrichment of interstellar methanol. By contrast, hydrogen sulfides undergo both H–D and D–H substitution on icy surfaces at 10 K (Figs. 5 and 8). In addition, the isotope effect is not significant ($k'/k'' \sim 1.4$). The atomic D/H ratio in dense clouds is generally much lower than unity (Roberts et al. 2004), implying that any deuterated sulfides formed by H–D substitution from H_2S are restored to H_2S through reactions with abundant H atoms on grains. This mechanism may in principle suppress the deuteration level of H_2S. However, once HDS is formed from H_2S via H–D substitution (reactions 5 and 6), it

may be released into the gas phase via chemical desorption. The desorbed HDS undergoes D–H substitution through reactions (14) and (15) only when re-adsorbed onto the grain surfaces, which might explain the relatively high deuteration levels of H_2S in the ISM.

5. Concluding Remarks

We experimentally demonstrated that H_2S can be released from various ice structures via chemical desorption at low temperatures. The effective desorption cross-section depends little on the ice structure and temperature. On the contrary, the degree of the desorbed fraction is influenced by both parameters, probably because the number and nature of the adsorption sites vary on ices with different textures. The present experimental results strongly suggest that the desorption efficiency per reactive event, which was estimated from the first linear part of the reaction, is much larger than that typically applied in modeling studies.

At 10 K, both H–D and D–H substitutions of hydrogen sulfides occur by tunneling atom-abstraction followed by barrierless atom addition. The isotope effect on the H–D and D–H substitution reactions was estimated from the ratio of the effective rate constants of the substitution reactions and the number density ratio of the D and H

atoms. The result was 1.4, meaning that the H–D substitution is slightly faster than D–H substitution on the p-ASW surface at 10 K. Note that the isotope effect was estimated on an assumption that the intermediate species HDS insignificantly contributed to the quantification of H_2S and D_2S. This small isotope effect excellently agreed with the theoretical value (also 1.4). Although the deuterated sulfides on grains will likely transform into their hydrogenated forms through D–H substitution, the deuteration levels of hydrogen sulfides in the gas phase may be maintained by chemical desorption upon the formation of deuterated sulfides.

Acknowledgment

The authors appreciated the consecutive review by an anonymous reviewer, which was helpful to improve the earlier version of the manuscript. The authors thank Dr. T. Lamberts at Leiden University, Dr. K. Furuya at University of Tsukuba, and Dr. W. M. C. Sameera at Hokkaido University for discussion on the surface reactivity and chemical desorption of H_2S. The authors also thank Dr. T. Hama at Hokkaido University for helpful comments on the preparation of H_2O ices. This work was partly supported by JSPS KAKENHI Grant Nos. JP26707030, JP17H06087, and JP17H04862.

Figure captions

Fig. 1 FTIR spectrum of solid H_2S (~0.7 ML) deposited on p-ASW (~30 ML) at 20 K (top), and the difference spectra after exposure to H atoms for 5 minutes (center) and 30 minutes (bottom).

Fig. 2 Relative abundances of solid H_2S on p-ASW versus atom exposure time at 10K (black), 20 K (red), and 30 K (blue). The solid lines are the least-squares fittings of the plots by Equation (4).

Fig. 3 TPD spectra (m/z = 34) of remaining solid H_2S after exposure to H atoms (a) at 20 K and (b) 30 K (solid red lines). The dashed lines are the TPD spectra obtained after exposure to H_2 molecules only (blank experiment) at each temperature.

Fig. 4 Relative abundances of solid H_2S on three kinds of ices (p-ASW, np-ASW, and c-H_2O) versus atom exposure time at 10 K.

Fig. 5 FTIR spectrum of solid H_2S (~0.7 ML) deposited on np-ASW (~30 ML) at 10 K (upper panel), and the difference spectra after exposure to D atoms for 20 s, 3 minutes, and 20 minutes (top to bottom in lower panel).

Fig. 6 Peak areas of the S–H stretching band of H_2S after exposure to D atoms on the three kinds of ices at 10 K. The values along the Y-axis are defined and interpreted in the main text. The solid lines are the least-squares fitting of the plots by Equation (10).

Fig. 7 Peak area of the S–D stretching band observed at 1860 cm^{-1} after exposure to D atoms on the three ice surfaces. The solid lines are guides for the eyes.

Fig. 8 (a) FTIR spectrum of solid D_2S (~0.7 ML) prepared on p-ASW-d (~30 ML) at 10 K, (b) difference spectra after exposure to H atoms for 3 minutes (top), 5 minutes (center), and 20 minutes (bottom), (c) difference spectrum of solid D_2S after exposure to H atoms for 80 minutes on Au substrate at 10 K (shown for comparison). The inset in (a) is an enlargement of the spectrum focusing on the S–D stretching band of D_2S (1860 cm^{-1}).

Fig. 9 Relative peak area of the S–D stretching band versus H-atom exposure time at 10 K (blue). The relative peak area of the S–H stretching band of H_2S after exposure to D atoms on p-ASW (black) is plotted for comparison. The solid lines are the least-squares fitting of the plots by Equation (10) or (16).

References

Chuang K.-J., Fedoseev G., Qasim D., Ioppolo S., van Dishoeck E. F., & Linnartz H. 2018, ApJ, 853, 102.
Collings M. P., et al. 2004, MNRAS, 354, 1133.
Coutens A., et al. 2012, A&A, 539, A132.
Coutens A., et al. 2014, ApJL, 792, L5.
Cuppen H. M., et al. 2017, SSRv, 212, 1.
Dulieu, F., et al. 2013, Sci. Rep. 3, 1338.
Fathe K., Holt J. S., Oxley S. P., & Pursel, C. J. 2006, J. Phys. Chem. A, 110, 10793.
Furuya K., Aikawa Y., Nomura H., Hersant F., & Wakelam V. 2013, ApJ, 779, 11.
Garrod, R. T., Wakelam, V. & Herbst, E. 2007, A&A, 467, 1103.
Geballe T. R., Baas F., Greenberg J. M., & Schutte W. 1985, A&A, 146, L6.
Hama T., Ueta H., Kouchi A., Watanabe N., & Tachikawa H. 2014, JPCL, 5, 3843.
Hatchell J., Thompson M. A., Millar T. J., & Macdonald G. H. 1998, A&A, 338, 713.
He J., Emtiaz S. M., & Vidali G. 2017, ApJ, 851, 104.
Hidaka H., Kouchi A., & Watanabe N. 2007, JCP, 126, 204707.
Hidaka H., Watanabe M., Kouchi A., & Watanabe N. 2009. ApJ, 702, 291.
Jiménez-Escobar, A. & Muñoz Caro, G. M. 2011, A&A, 536, A91.
Kimmel G. A., Stevenson K. P., Dohnálek Z., Scott Smith R., & Kay B. D. 2001, JCP, 114, 5284.
Kuwahata K., Hama T., Kouchi A., & Watanabe N. 2015, PRL, 115, 133201.
Lamberts T., & Kästner J. 2017, JPCA, 121, 9736.
Linsky, J. L. 2003, SSRv, 106, 49.
Millar T. J., Adams N. G., Smith D., Lindinger W., & Villinger H. 1986, MNRAS, 221, 673.
Millar T. J., & Herbst E. 1990, A&A, 231, 466.
Minh, Y. C., Irvine W. M., & Ziurys L. M. 1989, ApJL, 345, L63.
Minissale, M., Dulieu, F., Cazaux, S. & Hocuk, S. 2016, A&A, 585, A24.
Nagaoka, A., Watanabe, N., & Kouchi, A. 2007, JPCA, 111, 3016.
Neufeld D. A., et al. 2015, A&A, 577, A49.
Oba Y., et al. 2009, ApJ, 701, 464.
Oba Y., Osaka K., Watanabe N., Chigai T., & Kouchi A. 2014a, Faraday Discuss., 168, 185.
Oba Y., Chigai T., Osamura Y., Watanabe N., & Kouchi A., 2014b, MAPS, 49, 117.
Oba Y., Watanabe N., & Kouchi A. 2016a, Chem. Phys. Lett., 662, 14.

Oba Y., Osaka K., Chigai T., Kouchi A., & Watanabe N. 2016b, MNRAS, 462, 689.
Oba Y., Watanabe N., Hama T., Kuwahata K., Hidaka H., & Kouchi A. 2012, ApJ, 749,67.
Oba Y., Tomaru T., Lamberts, T., Kouchi A., & Watanabe N. 2018, Nat. Astron., 2, 228.
Parise B., et al. 2006, A&A, 453, 949.
Phuong N. T., et al. 2018, A&A, 616, L5.
Roberts H., Herbst E., Millar T. J., 2004, A&A, 424, 905.
Smith, R. G., Sellgren K., & Tokunaga A. T. 1989, ApJ, 344, 413.
Stevenson K. P., Kinmel G. A., Dohnálek Z., Scott Smith R., & Kay B. D. 1999, Sci., 283, 1505.
Taquet V., et al. 2013, A&A, 550, A127.
Thaddeus, P., Kutner M. L., Penzias A. A., Wilson R. W., & Jefferts K. B. 1972, ApJL, 176, L73.
van Dishoeck, E. F., Blake, G. A. Jansen, D. J. & Groesbeck, T. D. 1995, ApJ, 447, 760.
Vastel C., Phillips, T. G., Ceccarelli, C., & Pearson J. 2003, ApJL, 596, L97.
Vastel C., et al. 2010, A&A, 521, L31.
Wakelam V., et al. 2004, A&A, 413, 609.
Wakelam V., Loison J.-C., Mereau R., & Ruaud M. 2017, Mol. Astrophys., 6, 22.

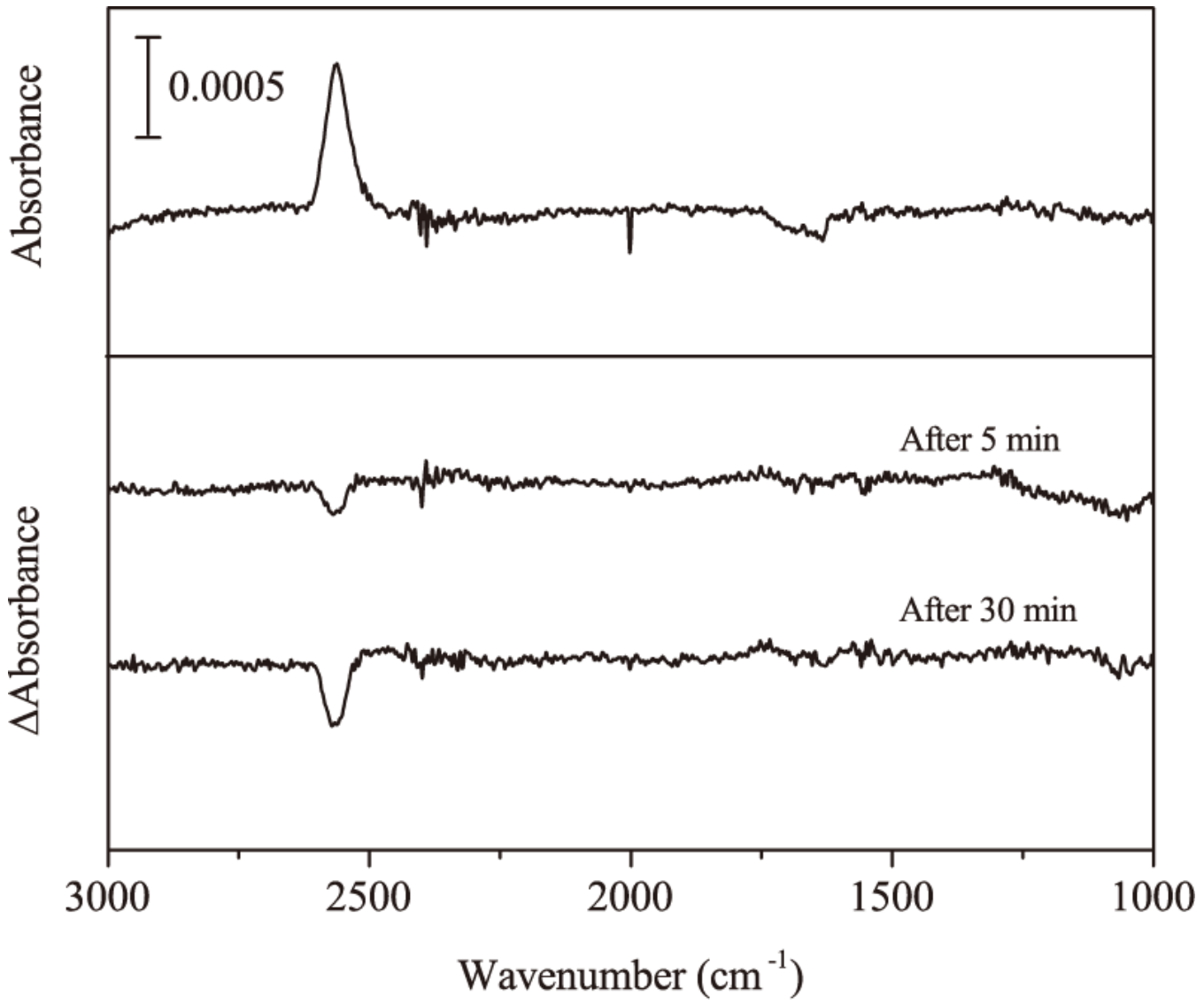
0.0005
Absorbance
After 5 min
After 30 min
ΔAbsorbance
3000
2500
2000
1500
1000
Wavenumber (cm -1)

Figure 1

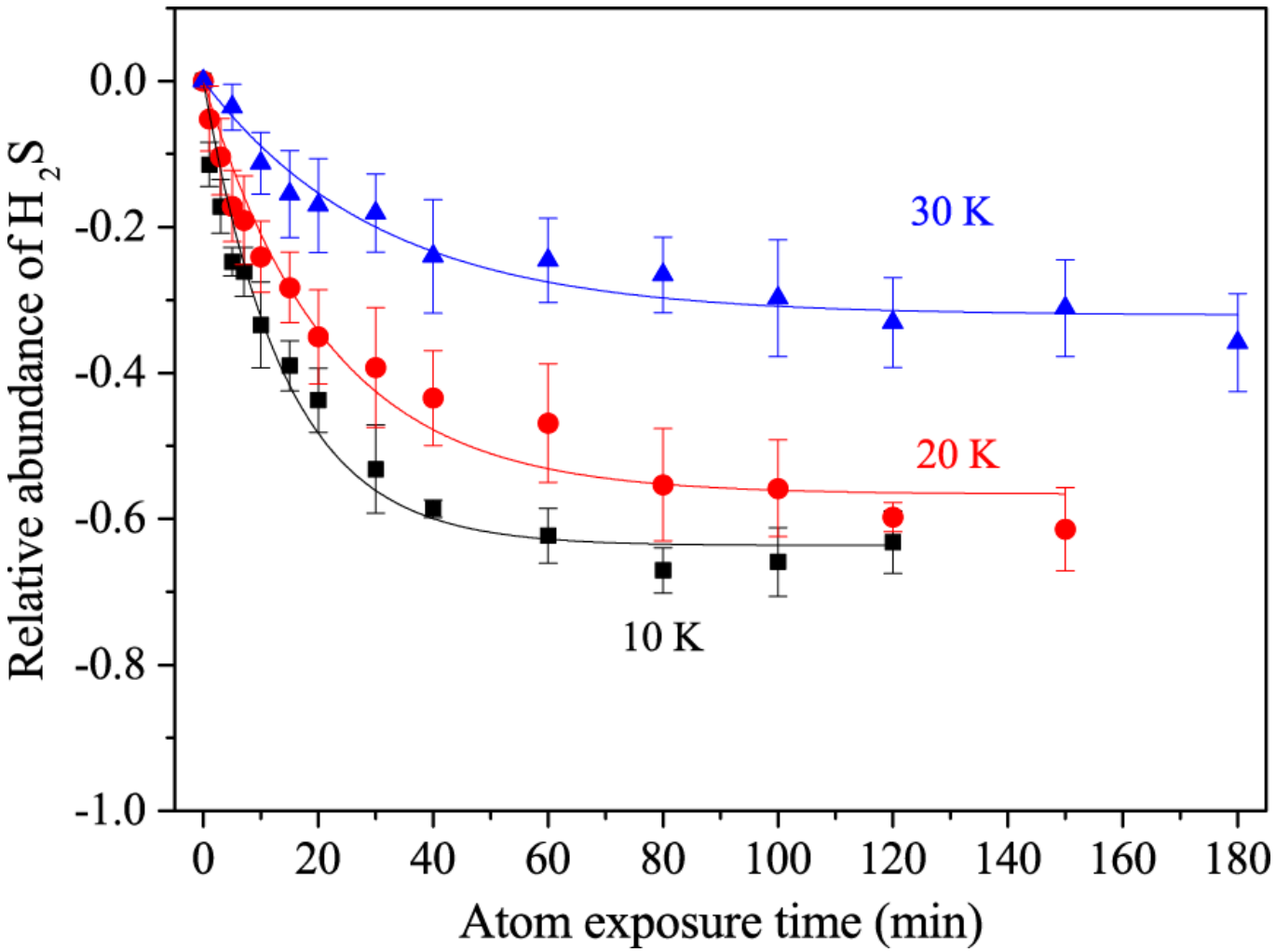
Relative abundance of H_2S
0.0
-0.2
-0.4
-0.6
-0.8
-1.0
0
20
40
60
80
100
120
140
160
180
Atom exposure time (min)
30 K
20 K
10 K

Figure 2

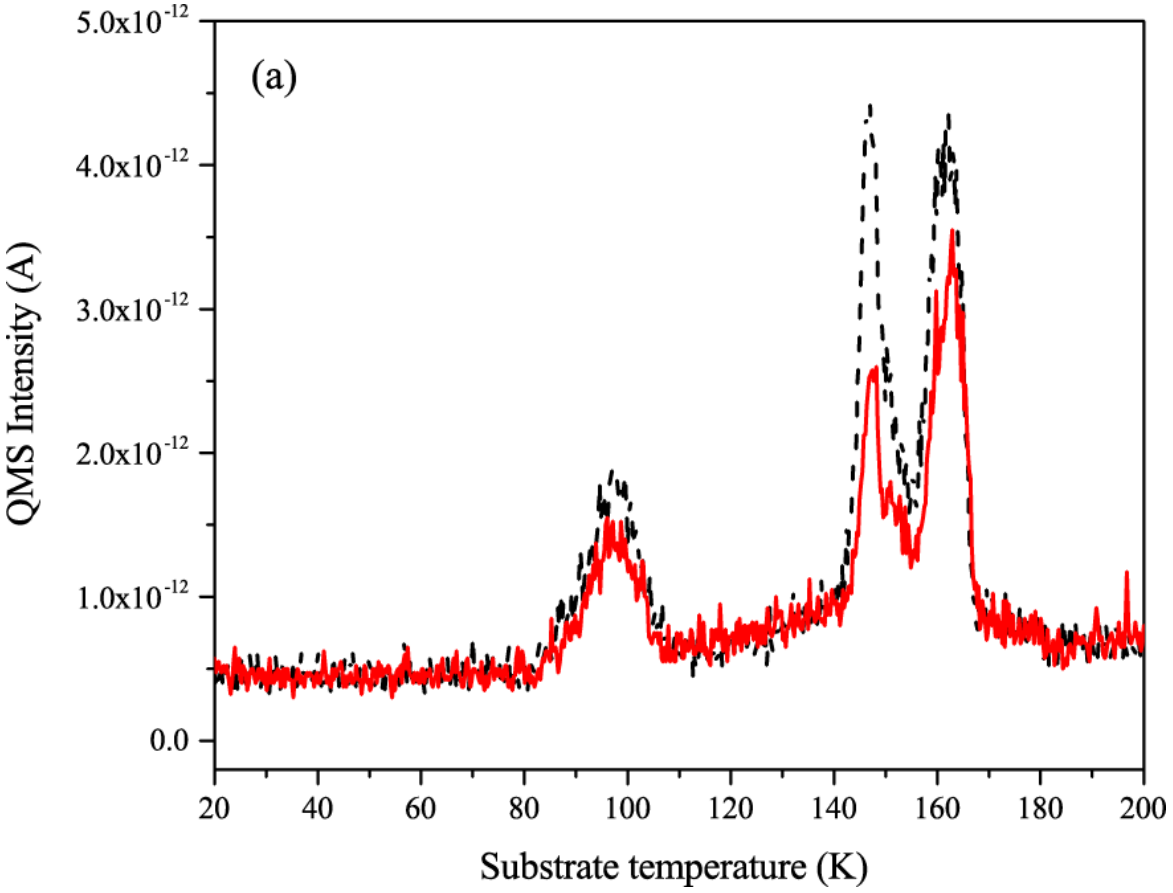
(a)
5.0x10-12
4.0x10-12
3.0x10-12
2.0x10-12
1.0x10-12
0.0
QMS Intensity (A)
20
40
60
80
100
120
140
160
180
200
Substrate temperature (K)

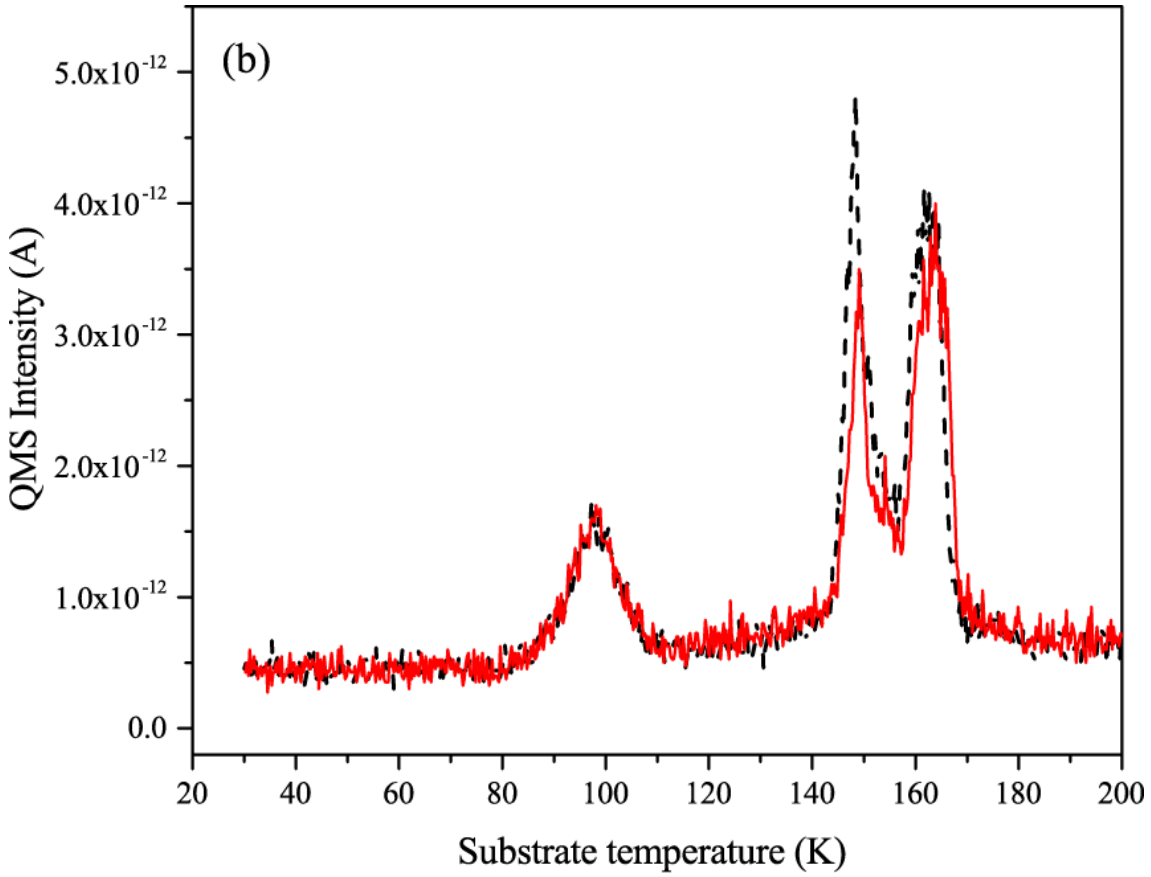
(b)
5.0x10-12
4.0x10-12
3.0x10-12
2.0x10-12
1.0x10-12
0.0
QMS Intensity (A)
20
40
60
80
100
120
140
160
180
200
Substrate temperature (K)

Figure 3

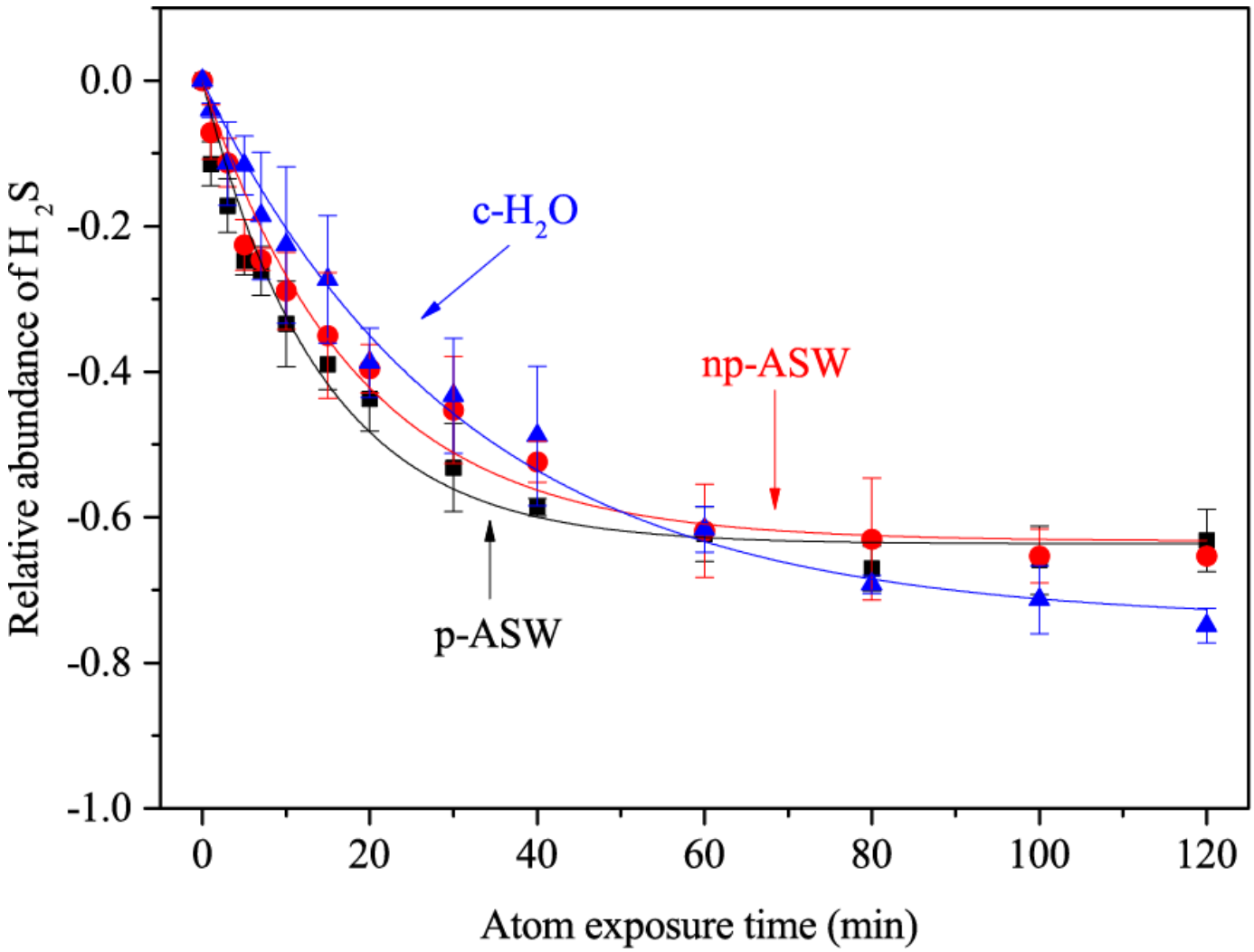
0.0
-0.2
-0.4
-0.6
-0.8
-1.0
Relative abundance of H 2S
c-H2O
np-ASW
p-ASW
0
20
40
60
80
100
120
Atom exposure time (min)

Figure 4

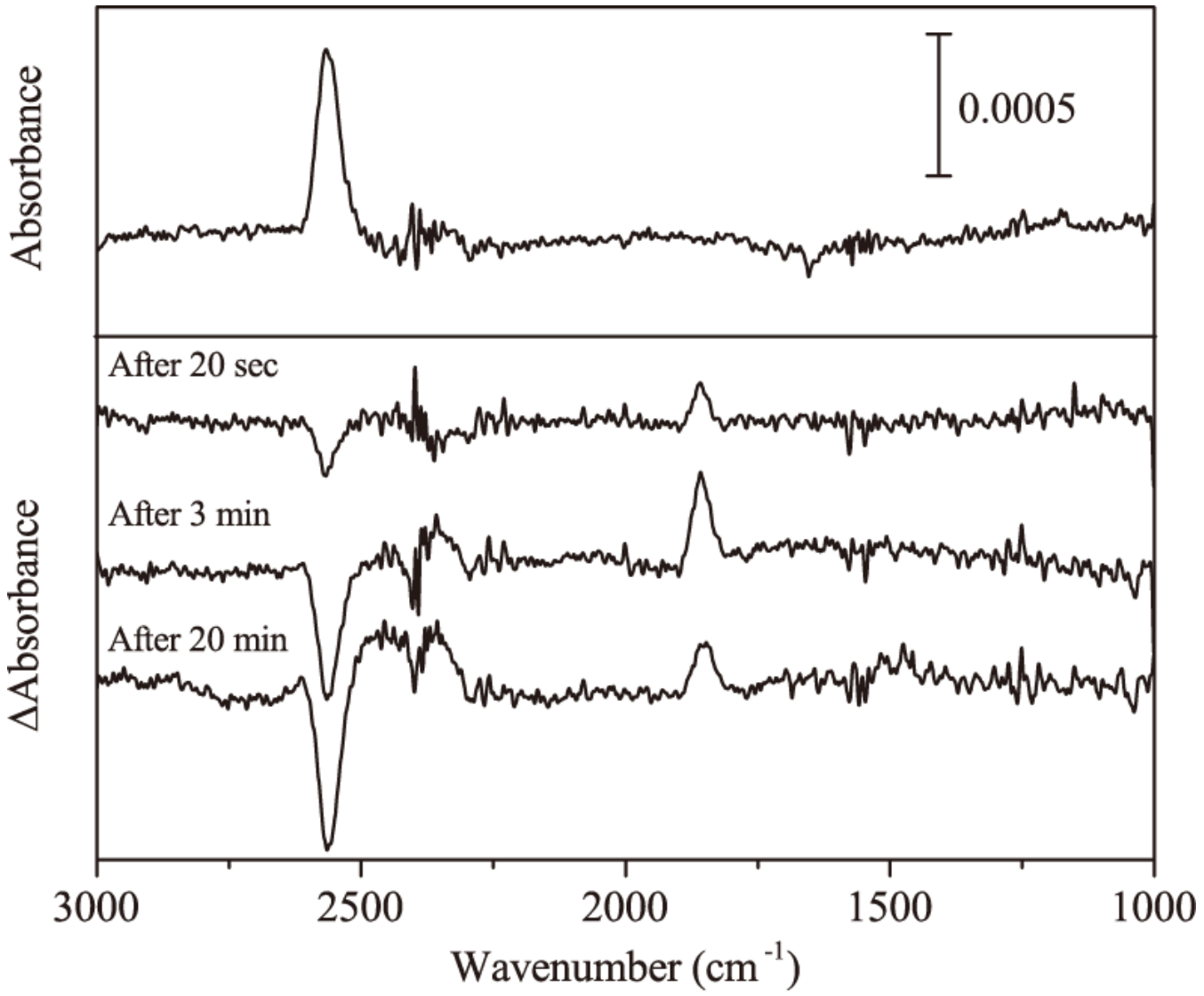
Absorbance
0.0005
After 20 sec
After 3 min
After 20 min
ΔAbsorbance
3000
2500
2000
1500
1000
Wavenumber (cm -1)

Figure 5

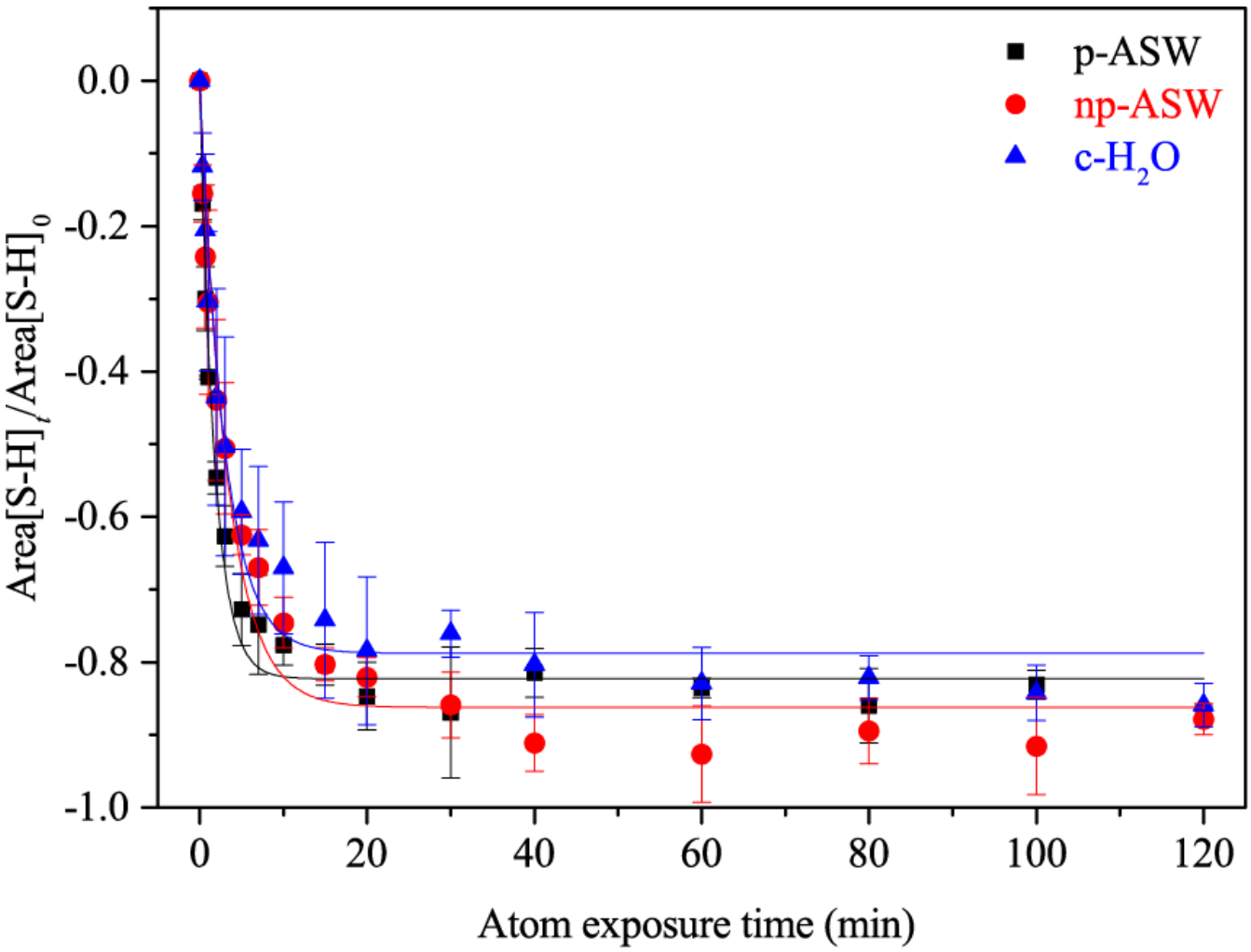
p-ASW
np-ASW
c-H2O
0.0
-0.2
-0.4
-0.6
-0.8
-1.0
Area[S-H]t/Area[S-H]0
0
20
40
60
80
100
120
Atom exposure time (min)

Figure 6

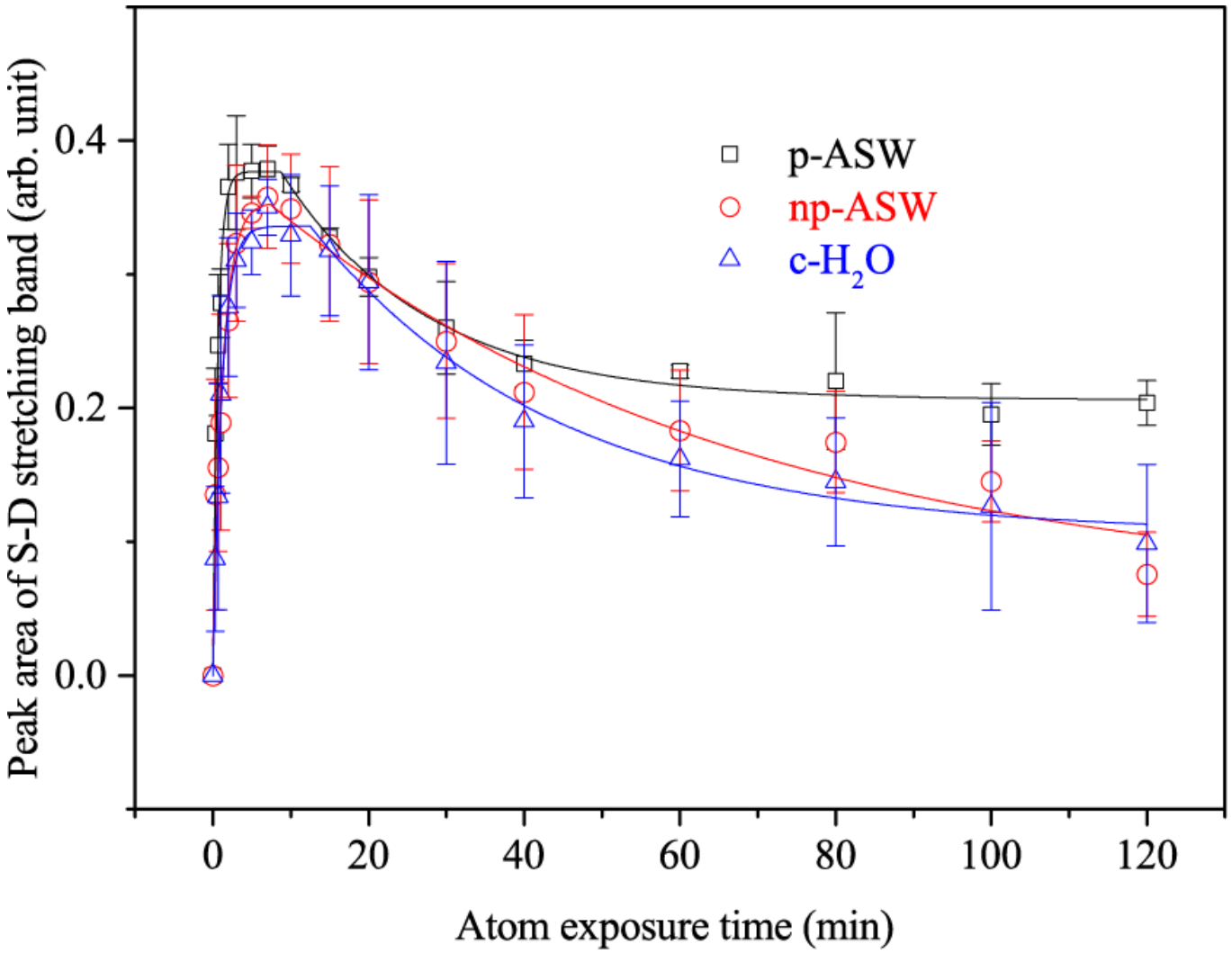
Peak area of S-D stretching band (arb. unit)
0.4
0.2
0.0
0
20
40
60
80
100
120
Atom exposure time (min)
p-ASW
np-ASW
c-H2O

Figure 7

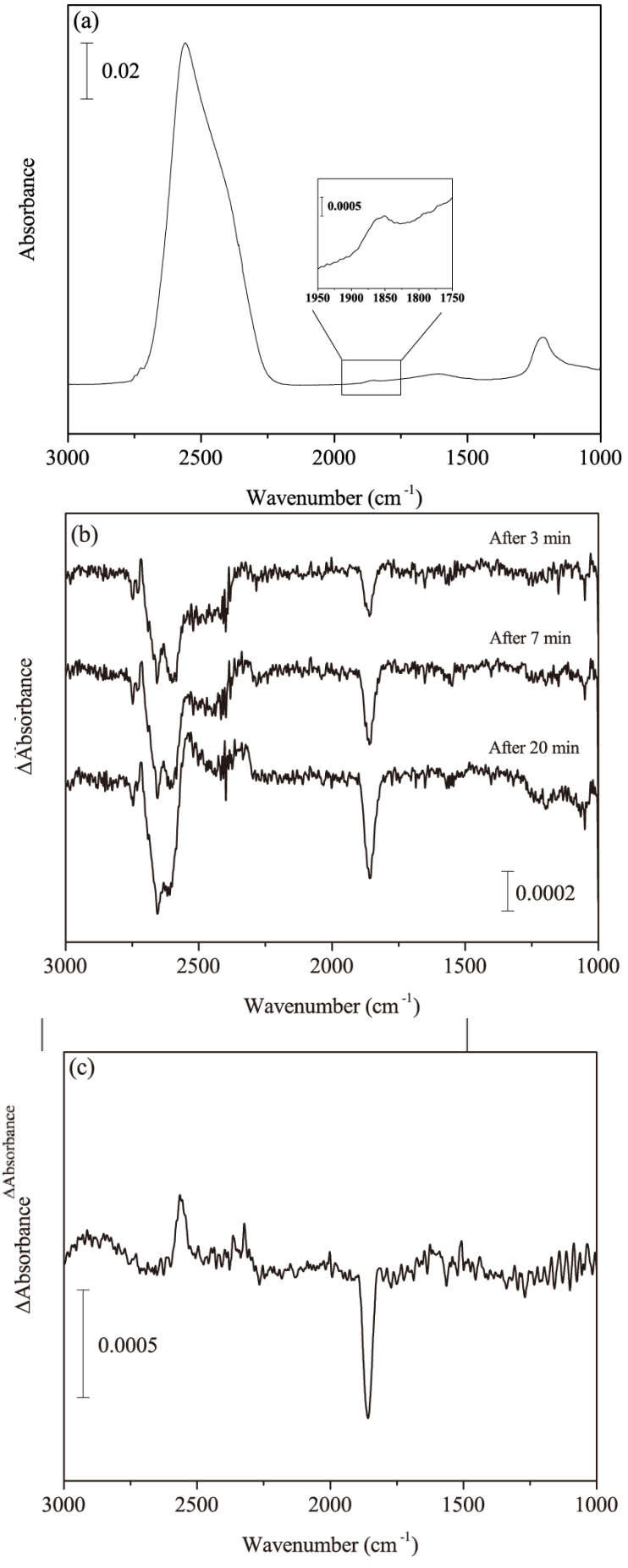
(a)
0.02
Absorbance
0.0005
1950 1900 1850 1800 1750
3000 2500 2000 1500 1000
Wavenumber (cm-1)
(b)
After 3 min
After 7 min
After 20 min
ΔAbsorbance
0.0002
3000 2500 2000 1500 1000
Wavenumber (cm-1)
(c)
ΔAbsorbance
ΔAbsorbance
0.0005
3000 2500 2000 1500 1000
Wavenumber (cm-1)

Figure 8

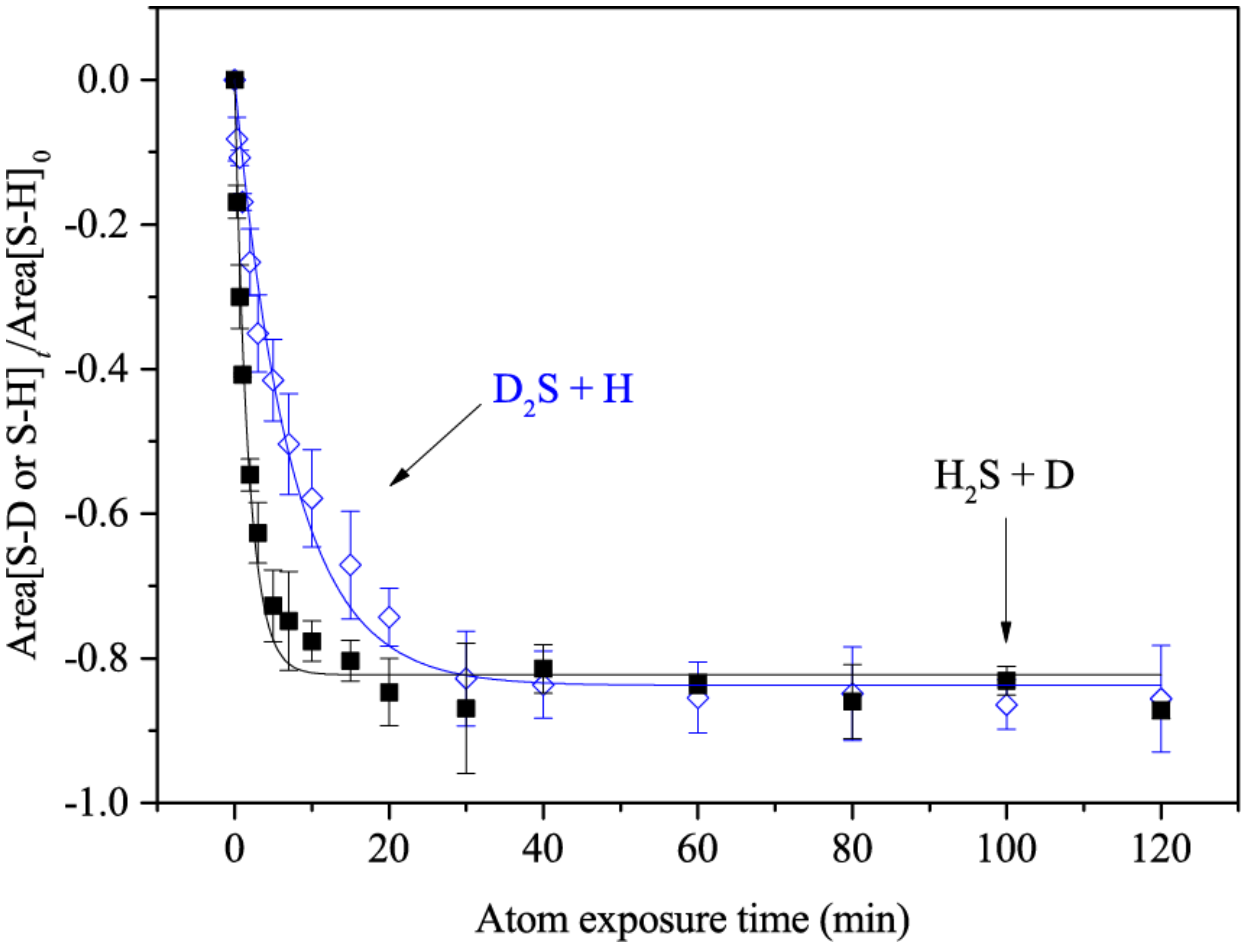
0.0
-0.2
-0.4
-0.6
-0.8
-1.0
Area[S-D or S-H] /Area[S-H]0
0
20
40
60
80
100
120
Atom exposure time (min)
D2S + H
H2S + D

Figure 9